Article



Multiscale mechanobiology: Coupling models of adhesion kinetics and nonlinear tissue mechanics

Yifan Guo, ¹ Sarah Calve, ^{2,3} and Adrian Buganza Tepole ^{1,2,*}

¹School of Mechanical Engineering, Purdue University, West Lafayette; ²Weldon School of Biomedical Engineering, Purdue University, West Lafayette; and ³Paul M. Rady Department of Mechanical Engineering, University of Colorado - Boulder, Boulder

ABSTRACT The mechanical behavior of tissues at the macroscale is tightly coupled to cellular activity at the microscale. Dermal wound healing is a prominent example of a complex system in which multiscale mechanics regulate restoration of tissue form and function. In cutaneous wound healing, a fibrin matrix is populated by fibroblasts migrating in from a surrounding tissue made mostly out of collagen. Fibroblasts both respond to mechanical cues, such as fiber alignment and stiffness, as well as exert active stresses needed for wound closure.

Here, we develop a multiscale model with a two-way coupling between a microscale cell adhesion model and a macroscale tissue mechanics model. Starting from the well-known model of adhesion kinetics proposed by Bell, we extend the formulation to account for nonlinear mechanics of fibrin and collagen and show how this nonlinear response naturally captures stretch-driven mechanosensing. We then embed the new nonlinear adhesion model into a custom finite element implementation of tissue mechanical equilibrium. Strains and stresses at the tissue level are coupled with the solution of the microscale adhesion model at each integration point of the finite element mesh. In addition, solution of the adhesion model is coupled with the active contractile stress of the cell population. The multiscale model successfully captures the mechanical response of biopolymer fibers and gels, contractile stresses generated by fibroblasts, and stress-strain contours observed during wound healing. We anticipate that this framework will not only increase our understanding of how mechanical cues guide cellular behavior in cutaneous wound healing, but will also be helpful in the study of mechanobiology, growth, and remodeling in other tissues.

SIGNIFICANCE Understanding how tissue mechanics and cellular activity are linked is key for improving treatment of diseases or injuries in which mechanical function is paramount, for example, in cutaneous wound healing. Previous mathematical models have described the spatiotemporal stresses, deformations, and change in mechanical properties of the healing wound by relying on phenomenological assumptions. A more detailed understanding of how fibroblasts sense and respond to mechanical cues by remodeling and exerting stress on the extracellular environment is needed to enable the next generation of wound healing treatments. This study addresses this gap by establishing a multiscale modeling framework that bridges our knowledge of cell adhesion at the microscale to the tissue mechanics at the macroscale.

INTRODUCTION

Mechanobiology is the study of how mechanical inputs, such as strain or stiffness of the extracellular matrix (ECM), affect the behavior of cells (1). The ability of cells to sense changes in the mechanical environment is essential for morphogenesis, maintenance of homeostasis, tissue growth, and remodeling. There are several mechanisms cells use for mechanosensing, including cell adhesions, cilia response to flow, and ion channels (2). For connective tissue cells, such as fibroblasts, and re-

Submitted August 19, 2021, and accepted for publication January 18, 2022.

*Correspondence: abuganza@purdue.edu

Editor: Vivek Shenoy.

https://doi.org/10.1016/j.bpj.2022.01.012

© 2022 Biophysical Society.

ceptors, such as integrins, are a critical component of how cells bind to specific ligands in the ECM and sense mechanical inputs (3,4). However, it is still unclear how forces and deformations at the macroscopic tissue scale, on the order of $\sim 10^{-1}$ m, are transferred to the cells at the microscale, on the order of $\sim 10^{-6}$ m. This problem is not trivial because cells are not rigidly attached to the ECM (5). Therefore, a proper understanding of tissue mechanics and mechanobiology necessitates multiscale models that couple adhesion kinetics between cells and the ECM at the microscale to deformation and stress of the tissue at the macroscale.

Cell-cell and cell-ECM adhesion were first described mathematically by Bell half a century ago (6). The core idea of this cell-ECM adhesion model is that integrin-ligand



bond kinetics have an intrinsic association rate, but the dissociation rate is based on a Boltzmann probability distribution with an exponential dependence on the energy at the adhesion. This model has since been advanced to capture the effect of elastic (7) and viscoelastic (8) properties of the substrate. The elastic model has shown that, other variables being the same, stiffer substrates favor cell adhesion and traction, which is consistent with the broad observation that cells spread and exhibit durotaxis in stiffer substrates (9–11). Consideration of viscoelasticity in the model suggests that the apparent stiffness sensed by cells is actually larger than the equilibrium stiffness of the substrate. This occurs because the energy in linear viscoelastic substrates is initially stored but then dissipated (8,12). Overall, the model originally proposed by Bell has continued to have success in modeling the adhesion of several cell types to a variety of substrates (7,8,13). However, the assumption of linear elastic or linear viscoelastic behavior of the ECM is too simplistic. The ECM is comprised of interpenetrating networks of proteins and glycosaminoglycans, the composition and organization of which vary depending on tissue type and pathological states (14), which leads to the nonlinear mechanical behavior of biological materials. For example, fibrin and type I collagen are two important biopolymers that contribute to the mechanical integrity of tissues and are particularly important during wound healing. Type I collagen and fibrin fibers and networks behave nonlinearly when deformed, with a characteristic strain-stiffening curve (15–18). The effect of this nonlinearity on fibroblast adhesion and traction has not been studied in detail. However, based on the evidence that stiffness and viscoelasticity affect fibroblast adhesion and traction, as well as evidence that fibrin and type I collagen exhibit nonlinear mechanics, we hypothesized that this nonlinearity would contribute to spatially heterogeneous traction by fibroblasts during wound healing.

Cellular adhesion and activity at the microscopic scale are eventually coupled to the mechanics of the tissue. To develop a model that integrates the macro- and microscales, we focused on changes that occur during cutaneous wound healing. Type I collagen is the primary load-bearing component of native skin (19). Upon injury, the first stage of wound healing is the formation of a provisional fibrin matrix at the site of injury (20,21). In many cases, connective tissues are under a prestrain, including skin (22). Moreover, during wound healing, contractile forces of individual fibroblasts are integrated across scales to produce active stress needed for wound contraction (23,24). Thus, the mechanical environment at and around the wound is complex. The heterogeneity given by the two different materials (i.e., the provisional fibrin matrix and surrounding collagenous tissue), the geometry of the wound, and the nonlinearity of the material itself, means that homogeneous models at the tissue scale are not enough to understand how mechanical inputs coordinate cellular activity. Instead, finite element models are a preferred tool to describe tissue mechanics at the macroscopic scale. Models of cutaneous wound healing mechanics are prevalent, including our own previous work (19,25–27). Recent efforts in computational modeling of wound healing have started to incorporate aspects of fibroblast mechanobiology (25,28); however, these models have relied on phenomenological assumptions. A better understanding of wound healing requires multiscale coupling between finite element models of tissue mechanics to the cell-level models of adhesion.

To address this gap, we extended existing models of cell adhesion at the microscale (6) to account for the nonlinear mechanics of fibrin and type I collagen (15–18). We show that the nonlinear stress-strain response of type I collagen and fibrin naturally lead to variation in the cell adhesion response. The behavior of cells and ECM were scaled up to the tissue level to capture the mechanics of tissue constructs through a custom finite element implementation. We anticipate that this work will lead to a better understanding of how tissue-level deformations are connected to cell mechanosensing, bridging, and expanding current biophysics models of tissue growth and remodeling.

MATERIALS AND METHODS

Adhesion model

We started with the well-known model of cell adhesion proposed Bell (6). Fig. 1 a illustrates the receptor-ligand interactions between the cell and the substrate as first-order reactions. Assuming the association process is intrinsic and independent of the mechanical properties of cells and the ECM, $k_{\rm on}$ is often considered as a constant, typically within the range of $0.002-0.3~{\rm s}^{-1}(29-31)$. In this work, the association rate was chosen to be $k_{\rm on}=0.002~{\rm s}^{-1}(29)$. The kinetic dissociation rate in Bell's adhesion model is defined by a Boltzmann distribution

$$k_{\rm off} = \hat{k}_{\rm off} e^{\Delta E/k_B T},$$
 (1)

where $\hat{k}_{\rm off}$ is the dissociation rate in the absence of force and can range from 10^{-5} to $0.012~{\rm s}^{-1}$ (29,31, k_B is the Boltzmann constant, T is the temperature in Kelvin, and ΔE is the energy stored at the adhesion.

In the traditional formulation of Bell's model, ΔE is calculated by the multiplication of a force applied to the bond and a transition distance (32). We compute this energy directly based on the deformation of the ECM to account for the nonlinear mechanical behavior of the ECM, as will be shown later. First, a Monte Carlo method was implemented in which a set of possible pairs of integrins and ligands were simulated independently. We then derived the approximating ordinary differential equation (ODE) from the limit of integrins and ligands approaching infinity. For the Monte Carlo and ODE simulations, the energy ΔE was computed assuming linear elastic and viscoelastic models before the problem was extended to the nonlinear mechanics regime.

Linear elastic and viscoelastic response

For the linear elastic (le) case, the energy stored at the adhesion is described by

$$\Delta E_{\rm le} = f \gamma = \frac{f^2}{2k_{\rm FCM}} \,, \tag{2}$$

where γ is a length scale parameter, f is the contractility force, and k_{ECM} is the ECM stiffness (6,7,13). For linear-viscoelasticity (lv), the energy at the

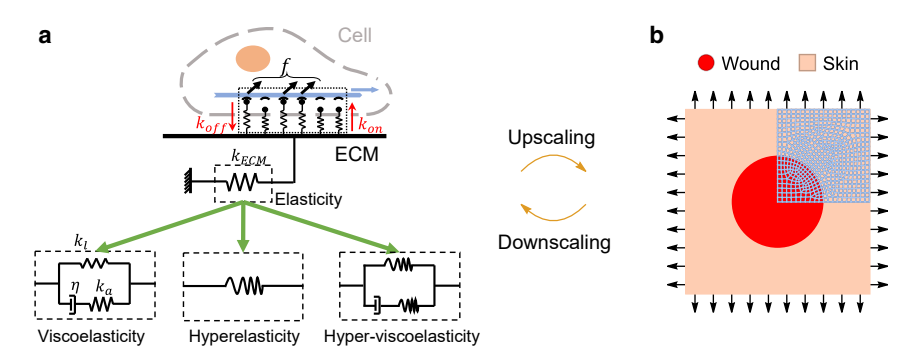


FIGURE 1 Schematic of microscale and macroscale models coupled in this study. (a) Microscale adhesion model. A cell illustrated by the gray dashed curve interfaces to the ECM through receptors that adhere to the ligands on the ECM. Each ligand can be represented by a spring that associates with a receptor with rate $k_{\rm on}$. Once a receptor-ligand pair is formed, the bond breaks at a rate $k_{\rm off}$, influenced by the contractile force f. The mechanics of the ECM can be captured with simplified models, such as linear elastic (depicted as a linear spring in the "elasticity" box in the figure), or linear viscoelastic ("viscoelasticity" box with a Maxwell represented the study of the contraction of the figure).

sentation of a standard linear solid). More realistic frameworks for ECM mechanics are those of "hyperelasticity" and "hyper-viscoelasticity" (represented as combinations of nonlinear springs and dashpots). (b) A simplified macroscale cutaneous wound domain. A round wound (red) embedded in a rectangular skin patch (pink). In vivo, skin is typically under a biaxial prestrain. The whole domain has two axes of symmetry. Only the top right quadrant was discretized with a finite element mesh. The cell-level model (a) can be upscaled to the tissue level (b) by homogenization based on the volume fraction of cells and ligands. The deformation at the tissue level (b) can be downscaled to the cell level (a) by considering the stretch of individual fibers in Eq. 4.

adhesion is a function of time from the moment a bond is formed. A Maxwell element is considered (Fig. 1 a), with stiffness k_l , additional stiffness k_a , and viscosity η . At the moment a bond forms, the single Maxwell element follows the time evolution

$$\Delta E_{\rm lv}(t) = \frac{f^2}{2k_l} + \frac{f^2 k_a e^{-\frac{2k_a k_l}{\eta(k_a + k_l)}t} \left(2e^{\frac{k_a k_l}{\eta(k_a + k_l)}t} - 1\right)}{2k_l (k_a + k_l)} \ . \tag{3}$$

Nonlinear elastic and viscoelastic response

For the nonlinear elastic and viscoelastic cases, we propose hyperelastic and hyper-viscoelastic models motivated by the Holzapfel-Gasser-Ogden model of soft tissues (33,34), and by previous work on fibrin and type I collagen gel mechanics (35–38). For simplicity, type I collagen is referred to as "collagen" for the rest of the manuscript. The strain energy density of a fiber network of $n_{\rm f}$ fibers is modeled with

Defining a relaxation time τ for the viscous branch (34), the time derivative of the elastic fourth invariant I_{4e} can be computed by

$$\dot{I}_{4e} = \frac{\frac{1}{\tau} \psi_{4e}^{f} I_{4e}}{\psi_{4e4e}^{f} I_{4e} + \psi_{4e}^{f}},\tag{5}$$

where

$$\psi_{4e}^{f} = \frac{\partial \psi^{f}}{\partial I_{4e}}, \quad \psi_{4e4e}^{f} = \frac{\partial^{2} \psi^{f}}{\partial I_{4e}^{2}}. \tag{6}$$

Thus, Eq. 5 is used to evolve the viscous branch in the nonlinear model. Given the total strain energy density function for the nonlinear case, we can compute the increase in energy at an adhesion as a result of the contractile force f. For the purely hyperelastic (he) case (i.e., no viscous branch, $\beta=0$ in Eq. 4), the energy at the adhesion becomes

$$\psi^{f}(I_{4}^{i}, I_{4e}^{i})$$

$$= \underbrace{\begin{cases} \frac{1}{n_{\mathrm{f}}} \sum_{i=1}^{n_{\mathrm{f}}} \frac{k_{1}}{2k_{2}} \left[e^{k_{2}(I_{4}^{i}-1)} - k_{2}(I_{4}^{i}-1) - 1 \right] & \text{if} \quad I_{4}^{i} \geq 1 \\ 0 & \text{if} \quad I_{4}^{i} < 1 \\ \frac{1}{n_{\mathrm{f}}} \sum_{i=1}^{n_{\mathrm{f}}} \frac{\beta k_{1}}{2k_{2}} \left[e^{k_{2}(I_{4e}^{i}-1)} - k_{2}(I_{4e}^{i}-1) - 1 \right] & \text{if} \quad I_{4e}^{i} \geq 1 \\ 0 & \text{if} \quad I_{4e}^{i} < 1 \end{cases} }$$

$$(4)$$

$$+ \underbrace{\begin{cases} \frac{1}{n_{\mathrm{f}}} \sum_{i=1}^{n_{\mathrm{f}}} \frac{\beta k_{1}}{2k_{2}} \left[e^{k_{2}(I_{4e}^{i}-1)} - k_{2}(I_{4e}^{i}-1) - 1 \right] & \text{if} \quad I_{4e}^{i} \geq 1 \\ 0 & \text{if} \quad I_{4e}^{i} < 1 \end{cases} }_{\text{viscoelastic component}}$$

The contribution of each fiber has an equilibrium elastic component and a viscoelastic component. The equilibrium strain energy density of the i^{th} fiber is in terms of the square of the total fiber stretch, I_4^i , while the viscous branch contributes to the strain energy density through the elastic component only I_{4e}^i . The parameters for the fiber strain energy density are a coefficient of the stiffness k_1 , a coefficient of nonlinearity k_2 , and a coefficient of viscosity β .

$$\Delta E_{\rm he}(\lambda) = (\psi(\tilde{\lambda}) - \psi(\lambda)) \cdot A \cdot l_0 , \qquad (7)$$

where $\lambda = \sqrt{I_4}$ is the stretch of the substrate, A is the cross-sectional area of a fiber, l_0 is a characteristic length related to the distance between two

adjacent ligands or integrins, and $\tilde{\lambda}$ is the new total stretch of the substrate under a constant cellular contractile force f.

For the hyper-viscoelastic (hv) case, β >0, the energy in each adhesion depends not only on the stretch but also on the time since the bond is formed.

$$\Delta E_{\rm hv}(\lambda, t) = (\psi(\tilde{\lambda}, t) - \psi(\lambda)) \cdot A \cdot l_0. \tag{8}$$

As opposed to the linear viscoelastic case in Eq. 3, there is no closed-form solution for Eq. 8.

Monte Carlo simulations

Cell adhesion is simulated by first considering an array of individual ligandreceptor pairs. The association and dissociation processes can be considered as a Poisson process. The probabilities of single association and dissociation in every time increment can be written as

$$P_{\text{on},0} = 1 - e^{-\Delta t \, k_{\text{on}}} \,, \tag{9}$$

$$P_{\rm off} = 1 - e^{-\Delta t \, k_{\rm off}} \,. \tag{10}$$

Taking into consideration the density of bonds, $r_{\rm RL}$ as in (39), the probability of forming a bond is

$$P_{\rm on} = 1 - (1 - P_{\rm on \, 0})^{r_{\rm RL}} \,. \tag{11}$$

The dissociation rate, $k_{\rm off}$ defined in Eq. 1 depends on the energy at the adhesion, and, depending on the model of the ECM mechanics, is given by Eqs. 2, 3, 4, 5, 6, 7, and 8. Note that when viscoelasticity is considered, the $k_{\rm off}$ rate is time dependent (refer to Eqs. 3 and 8), requiring internal variables to keep track of the time at which a receptor-ligand pair is formed. The material parameters are specific to each model; however, all Monte Carlo simulations use the same range of contractile forces, from 2.2-35.6 pN(40). We chose f=7 pN(40). Table S1 summarizes all the parameter values.

The number of bonds at $t_{n+1} = t_n + \Delta t$ can be computed based on

$$N_{n+1} = P_{\text{on}}(N_{\text{max}} - N_n) - P_{\text{off}}N_n \tag{12}$$

where N_{n+1} and N_n denote the number of existing bonds at next time increment and at the current time, respectively, and $N_{\rm max}$ denotes the total number of possible bonds, i.e., the total number of possible receptor-ligand pairs in the Monte Carlo simulation.

ODE limit

As the number of receptors grows, the total number of receptor-ligand bonds can be approximated by the ODE

$$\dot{\varphi}_b = r_{\rm RL} k_{\rm on} (1 - \varphi_b) - k_{\rm off} \varphi_b , \qquad (13)$$

where φ_b denotes the density of the receptor-ligand bonds. Note that $k_{\rm off}$ in the ODE captures an average response from all receptor-ligand bonds. The dissociation rate is a constant for the linear elastic case, and it only depends on the initial stretch of the substrate for the hyperelastic case. However, in the linear viscoelastic and hyper-viscoelastic cases, the dissociation rate is time dependent for an individual bond. Thus, for the ODE we need to determine an average relaxation time. This can be derived from the analysis of the nonhomogeneous Poisson process. The relaxation time, $\tau_{\rm off}$ is based on

$$\tau_{\text{off,avg}} = \frac{\int_0^{\tau_{\text{off}}} t P_{\text{off}}(t) dt}{\int_0^{\tau_{\text{off}}} P_{\text{off}}(t) dt}, \qquad (14)$$

where

$$P_{\text{off}}(t) = \exp\left(-\int_0^t \widehat{k}_{\text{off}} e^{\frac{\Delta E(s)}{k_B T}} ds\right), \tag{15}$$

$$\tau_{\text{off}} = \frac{(k_l + k_a)\eta}{k_l k_a} \log\left(\frac{1 + \sqrt{CI}}{1 - CI}\right), \tag{16}$$

with CI the confidence interval assumed in the averaging. In our simulation we choose CI=0.99.

Macroscale response of biopolymer gels

Considering that the ECM in native tissues contains multiple materials besides collagen and fibrin fibers, we treat the ECM as a fiber-reinforced composite, where the fibrillar proteins are the "fibers" and the amorphous, glycosaminoglycan-rich, ground substance as the "matrix." The fibers are scaled by a volume fraction ζ_f . The total strain energy density function can be written as

$$\psi(I_1, I_4, I_{4e}, J) = \underbrace{\psi^{\mathrm{m}}(I_1)}_{\text{isotropic matrix}} + \underbrace{\zeta_{\mathrm{f}} \psi^{\mathrm{f}}(I_4, I_{4e})}_{\text{anisotropic fiber}} + \underbrace{\psi^{\mathrm{vol}}(J)}_{\text{volumetric term}},$$
(17)

which is the sum of an isotropic ground substance contribution (ψ^m) , a weighted anisotropic fiber contribution $(\zeta_f \psi^f)$, and a volumetric term (ψ^{vol}) to capture compressibility or enforce incompressibility. The isotropic contribution is dictated by the deformation invariant I_1 , and parameterized by k_0 , i.e.,

$$\psi^{\rm m}(I_1) = k_0(I_1 - 3). \tag{18}$$

Even though soft tissues are often treated as incompressible (19), experimental evidence indicates that collagen and fibrin gels can be compressible (41,42). Implementation of compressible volumetric terms as described in (41,42) is reported and discussed in the supporting material. However, compressibility based on (42), can cause nonconvex behavior and exhibit extreme sensitivity to parameters. Thus, to ensure convergence of the finite element simulations, we implemented the incompressible case; the volumetric term is given by

$$\psi^{\text{vol}}(J) = p(J-1) , \qquad (19)$$

where J is the volume change. The incompressibility condition J=1 is enforced by the pressure Lagrange multiplier p which can be solved analytically for plane stress two-dimensional problems (25).

Finite element model

The finite element code used in the study is a custom implementation in C++. Mechanical equilibrium is solved for by requiring the vanishing of the stress divergence

$$\nabla_{\mathbf{r}} \cdot \boldsymbol{\sigma} = 0. \tag{20}$$

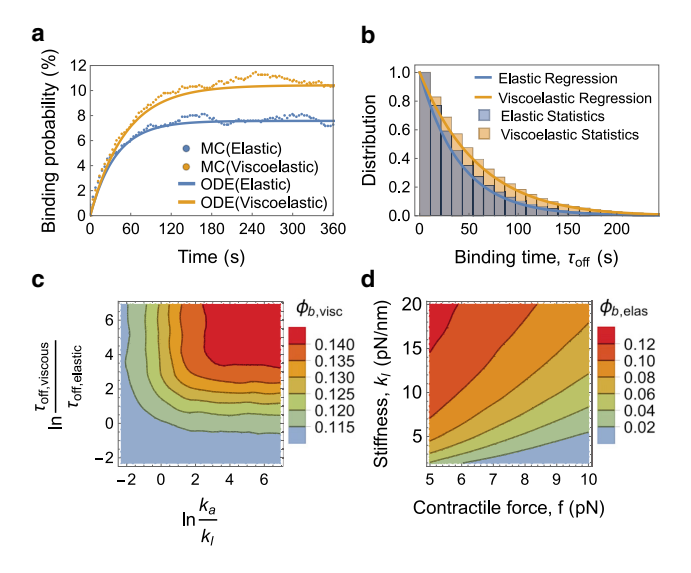


FIGURE 2 Linear elastic and linear viscoelastic models of adhesion. (a) Monte Carlo (MC) simulations and corresponding ODE simulations for adhesion processes on a purely elastic substrate and a viscoelastic substrate. The scatter points show the results from 10,000 MC steps. The binding probability was calculated by the ratio of the number of receptor-ligand bonds to the number of total receptor-ligand pairs. The solid lines show the results from the ODE model. (b) The histograms describe the distributions of the binding time of receptor-ligand pairs. The solid lines are the regression curves for the corresponding statistical data. The median relaxation time of the viscoelastic model used in the ODE was computed based on the statistics of $\tau_{\rm off}$. (c) The contour shows the influence of the additional stiffness in the Maxwell branch and the viscosity (represented by the relaxation time) on the binding probability. The reference timescale $au_{
m off,elas}$ was a characteristic unbinding time. (d) The contour shows the binding probability on a purely elastic substrate with respect to the contractile force and the stiffness of the substrate.

The total stress σ can be separated into two parts: the passive contribution σ^{pas} and the active contribution σ^{act} ,

$$\boldsymbol{\sigma} = \boldsymbol{\sigma}^{\text{pas}} + \boldsymbol{\sigma}^{\text{act}} \,. \tag{21}$$

The passive part of the stress considers isotropic and anisotropic contributions based on Eq. 17. The active part is the result of cell tractions and is introduced below.

The anisotropic term, Eq. 4 requires sampling multiple fiber orientations for $n_{\rm f}$ fibers, which can be done using Monte Carlo sampling. However, this approach results in excessive computational time. Alternatively, we select several primary orientations and compute the weighted mean of the strain energy density function according to the probability density of a von Mises fiber orientation distribution. Our code follows a total Lagrangian formulation based on the second Piola-Kirchhoff stress. The isotropic ground substance (m) component of the second Piola-Kirchhoff stress is

$$\mathbf{S}^{\text{pas,m}} = 2\psi_1^{\text{m}}\mathbf{I} + 2p\mathbf{C}^{-1}, \qquad (22)$$

where $\psi_1^{\rm m}$ denotes the first derivative of the isotropic part of the total strain energy density function with respect to the first invariant of deformation, I_1 , and the term including p is the volumetric stress. The tensor \mathbf{I} denotes the identity, C is the right Cauchy-Green deformation tensor. The anisotropic fiber (f) contribution is

$$\mathbf{S}^{\text{pas,f}} = 2\zeta_{\text{f}} \sum_{i=1}^{n_{\theta}} P(\theta_{i}) \left(\psi_{4,i}^{\text{f}} \mathbf{a}_{0i} \otimes \mathbf{a}_{0i} + \psi_{4e,i}^{\text{f}} \frac{I_{4e}^{i}}{I_{4}^{i}} \mathbf{a}_{0i} \otimes \mathbf{a}_{0i} \right),$$
(23)

where

$$\psi_{\alpha,i}^{\mathrm{f}} = \frac{\partial \psi^{\mathrm{f}}}{\partial I_{\alpha}^{i}}, \quad \alpha = 4, 4e,$$
(24)

 $P(\theta_i)$ is the probability of the i^{th} angle θ_i appearing according to von Mises distribution, and \mathbf{a}_{0i} is the orientation of the i^{th} fiber in the reference

The total second Piola-Kirchhoff stress is simply the sum

$$\mathbf{S}^{\text{pas}} = \mathbf{S}^{\text{pas,m}} + \mathbf{S}^{\text{pas,f}} + p\mathbf{C}^{-1} . \tag{25}$$

To represent the formulation in the current configuration, the push-forward of the stress is calculated by the deformation gradient F and the Jacobian J,

$$\boldsymbol{\sigma}^{\text{pas}} = \frac{1}{J} \boldsymbol{F} \cdot \boldsymbol{S}^{\text{pas}} \cdot \boldsymbol{F}^{\top} . \tag{26}$$

We introduce an active contribution of the total stress due to cell contractility. This active stress is naturally defined in the current configuration

$$\boldsymbol{\sigma}^{\text{act}} = \zeta_c \, t_{\rho}(\lambda) \sum_i \frac{\mathbf{a}_i \otimes \mathbf{a}_i}{tr(\mathbf{a}_i \otimes \mathbf{a}_i)} \,, \tag{27}$$

where ζ_c is the volume fraction of the cells and \mathbf{a}_i is the orientation of the i^{th} fiber in the current configuration. The traction produced by a single cell, $t_{\rho}(\lambda)$, is given directly as a function of force per receptor and the density of receptors, and indirectly as a function of the deformation via the adhesion model,

$$t_{\rho}(\lambda) = f \cdot \rho_r \cdot \varphi_b(\lambda) , \qquad (28)$$

where f is the contractile force per adhesion and ρ_r is the density of receptors per cell, the typical value of which is in the range of 300 μ m⁻² – 500 μm⁻²(39). Parameters of the finite element model are also summarized in Table S1.

RESULTS

Adhesion kinetics for the linear elastic and viscoelastic cases

For the Monte Carlo model, we assumed the initial states of all the receptor-ligand pairs were "off," tested a case of 1000 integrins in total, and simulated 3600 s with time step $\Delta t = 0.36$ s. We simulated both linear elastic and linear viscoelastic cases, and compared the results of the Monte Carlo method against those obtained with the ODE model in Fig. 2, a and b. The results of the Monte Carlo simulations matched the ODE. Note that in the Monte Carlo simulations the time it takes for every bond to dissociate is stored, $\tau_{\rm off}$ (Fig. 2 b), whereas the ODE method uses only the expected value of this

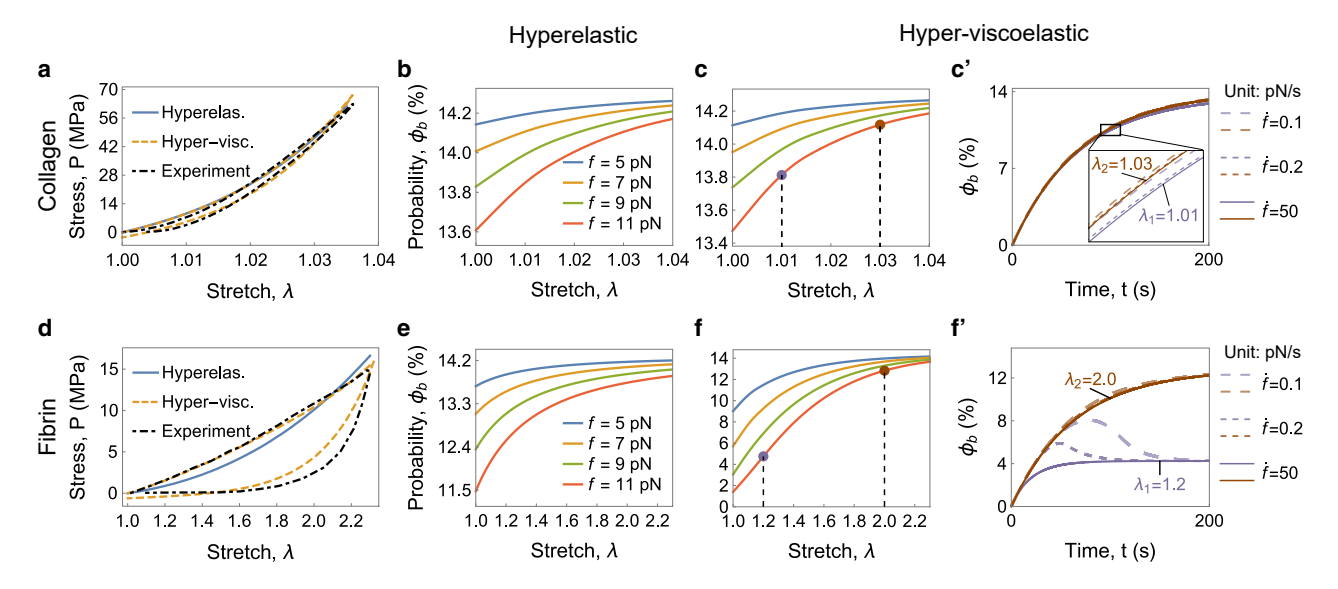


FIGURE 3 Effect of nonlinear mechanics of fibers on cell adhesion. Experimental nominal stress data for uniaxial tension tests of (a) single collagen (15) and (d) fibrin fibers (17) were used to obtain the parameters for the anisotropic part of the hyperelastic and hyper-viscoelastic models. The black dashed line shows the experimental data; the blue solid line shows the fit with the hyperelastic model; the orange dashed line shows the fit with the hyper-viscoelastic model. The changes of binding probability φ_b as a function of the stretch of (b) collagen fiber in the hyperelastic model, (e) fibrin fiber in the hyperelastic model, (c) collagen fiber in the hyper-viscoelastic model, and (f) fibrin fiber in the hyper-viscoelastic model under different contractile forces, f, are illustrated. The transient behavior of the adhesion probability and the influence of contractile force rate on fibers under different prestretch were further investigated. A relatively small prestretch (purple point) and a large prestretch (brown point) were chosen in c' and f', and three force loading rates were applied.

distribution. We computed the regression curve of $\tau_{\rm off}$ based on the theory of nonhomogeneous Poisson processes. The agreements of the regression curves and the statistical results allowed us to compute the average relaxation time of the viscoelastic model used in the ODE according to Eq. 14.

To better understand the relationship of the binding probability φ_b with respect to the relaxation time and the stiffness in the elastic and viscoelastic systems, we defined a characteristic time of dissociation for the purely elastic model $\tau_{\rm off,elastic}$ as

$$\tau_{\text{off,elastic}} = \frac{1}{\hat{k}_{\text{off}}}$$
 (29)

We then compared the probability of unbinding time in the viscoelastic case, $\tau_{\rm off}$, to the baseline time of the elastic case $au_{
m off,elastic}$. This ratio is proportional to the viscosity of the Maxwell branch. We also varied the ratio of the additional stiffness in the Maxwell branch to the long-term stiffness. We found that higher viscosity (higher $\tau_{\rm off}$) resulted in increasing binding probability. Similarly, increasing the additional stiffness also increased adhesion (Fig. 2 c), consistent with experimental observations (8). Subsequently, we analyzed the influence of the contractile force and the long-term stiffness (equilibrium stiffness of the ECM) on the binding probability. The contour is depicted in Fig. 2 d. The higher stiffness of the substrate improved the binding probability, increasing adhesion, and the larger contractility reduced that probability, which is consistent with experiments (43,44).

Nonlinear mechanics of the ECM leads to adhesion-mediated mechanosensing

Having verified that the linear models were consistent with the literature, we increased the complexity by incorporating nonlinearity. Equation 4 was fit to experimental data of collagen fibers (15) and fibrin fibers (17) (Fig. 3 a), accounting for, and ignoring, viscoelastic behavior. Both fits were able to capture the mechanical properties of collagen and fibrin fibers. Due to the intrinsic nonlinearity of the strain energy function, the model predicted changes of binding probability, φ_b , with respect to the stretch of the substrate (Fig. 3, a-f). Note that the adhesion model was solved following the stretch of the fiber. The collagen fiber is significantly stiffer than the fibrin fiber, so the change in φ_h with stretch for collagen was less than that for fibrin. In both cases, the nonlinearity in the mechanics is such that stretch led to an increase in binding probability, showing the mechanosensitivity of cell adhesion to ECM deformation. Increasing contractile forces, f, had the opposite effect (Fig. 3, b, c, e, and f), consistent with the fact that increasing force induces strain energy at the adhesion and thus increases the dissociation rate (45). For collagen, there were only small changes between the hyperelastic model and the hyper-viscoelastic model (Fig. 3, b and c). On the other hand, the viscous dissipation for fibrin was

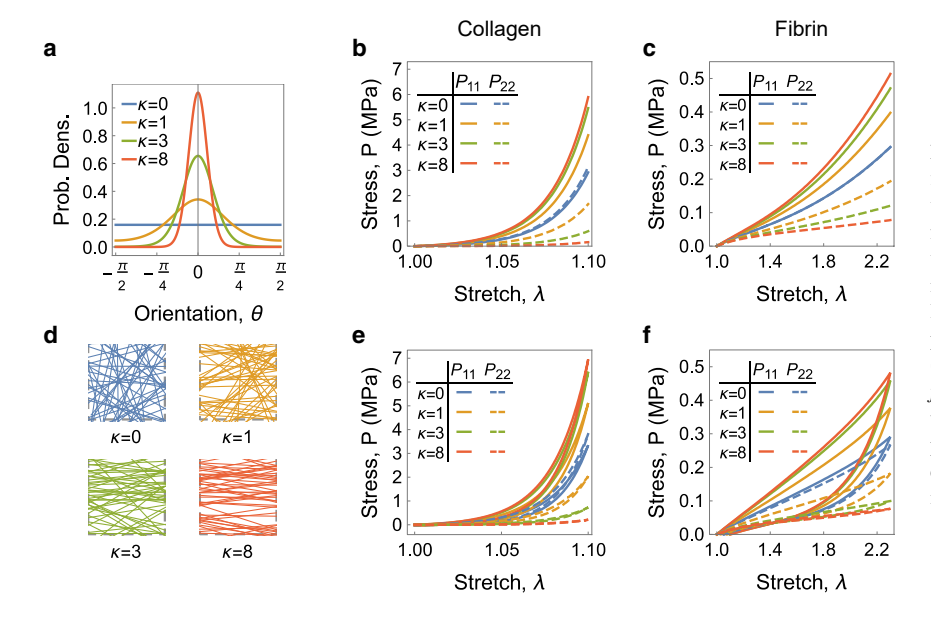


FIGURE 4 Passive response of collagen and fibrin gels. (a and d) A von Mises distribution was used to describe fiber orientation, with $\kappa = 0$ for the isotropic case and progressively larger values of κ to describe anisotropic gels. Fiber stiffness parameters were kept from the previous analyses of individual fiber data, but additional parameters for the gel response were based on (46) for collagen, and (48) for fibrin. (b, c, e, andf) Biaxial responses of gels were evaluated for (b) the collagen hyperelastic model, (c) the fibrin hyperelastic model, (e) the collagen hyper-viscoelastic model, and (f) the fibrin hyper-viscoelastic

large (Fig. 3 d). As a result, binding probability became extremely sensitive to stretch when the fibrin model was switched from hyperelastic to hyper-viscoelastic (Fig. 3, e and f). In Fig. 3 c and f only the equilibrium states are considered. However, contractile forces are highly dynamic, and this effect is important for the viscous fibers. Fig. 3, c' and f' show the time evolution of the adhesion probability for cells on collagen or fibrin for two different values of fiber prestretch and for three contractile force rates. For cells on collagen fibers, the transient evolution of the adhesion is not sensitive to fiber stretch or to contractile force rate due to the high stiffness of collagen. In contrast, for the fibrin fibers, which are softer, both the fiber stretch and contractile force rate have an influence on binding probability. When a fibrin fiber is stretched to a higher value, the tangent stiffness increases. As a result, the steady state of the adhesion model increases with prestretch of fibrin. This was already evident in Fig. 3 f, but Fig. 3 f' further illustrates the time evolution of the adhesion toward two different steady states depending on fiber stretch. The contractile force rate has an influence on the transient behavior. A slower contractile force rate leads to an overshoot in adhesion before the adhesion probability goes down to the equilibrium value. This is because the increase in contractile force increases the dissociation rate. By applying the contractile force gradually, the dissociation rate increases slowly and the resulting dynamic behavior is underdamped.

Homogeneous deformation of collagen and fibrin gels

After fitting the experimental data of single collagen and fibrin fibers, we fit the experimental data of collagen (46,47) and fibrin gels (48) to the nonlinear models (Eq.

17). These data allowed us to determine the isotropic parameter k_0 and volume fraction ζ_f . Parameters are summarized in Table S1. A von Mises distribution with parameter κ was used to describe different orientations. We chose four different orientations $\kappa = 0, 1, 3, 8$ to sample fiber directions (Fig. 4 a). We computed the stresses of collagen and fibrin gels under biaxial tension because it is more physiologically relevant than uniaxial tension (49), considering both hyperelastic and hyper-viscoelastic models (Fig. 4, b, e for collagen, Fig. 4, c, f for fibrin). The primary orientation of fibers was assumed to be along direction [1,0]. As expected, the more aligned the fibers were, the more stress was generated in the primary orientation, P_{11} , whereas the isotropic distribution $\kappa = 0$ led to an isotropic response, $P_{11} = P_{22}$. The stresses in collagen gels were an order of magnitude larger with respect to fibrin and the loading path was highly nonlinear for collagen but more linear for fibrin. The collagen gels exhibited much less viscous dissipation than fibrin gels. All of these observations are in alignment with the experimental data of both individual fibers and gels (15,17,46,48), and suggest that our constitutive models Eqs. 4 and 17 are suitable to describe the multiscale mechanics of collagen and fibrin.

Next, we focused on the active contribution of cells to the substrate (defined in Eq. 27). We continued to consider a homogeneous problem but this time assuming free boundary conditions in all directions. This type of problem is representative of gel contraction experiments to measure cell contractility (26,50,51). We investigated receptor density, contractility, and characteristic length (a reference length between two receptors) separately to determine the influence of those three parameters on the overall contraction of collagen and fibrin gels. Increasing receptor density ρ_r (Fig. 5, a and d) and contractility f (Fig. 5, b and e) induced

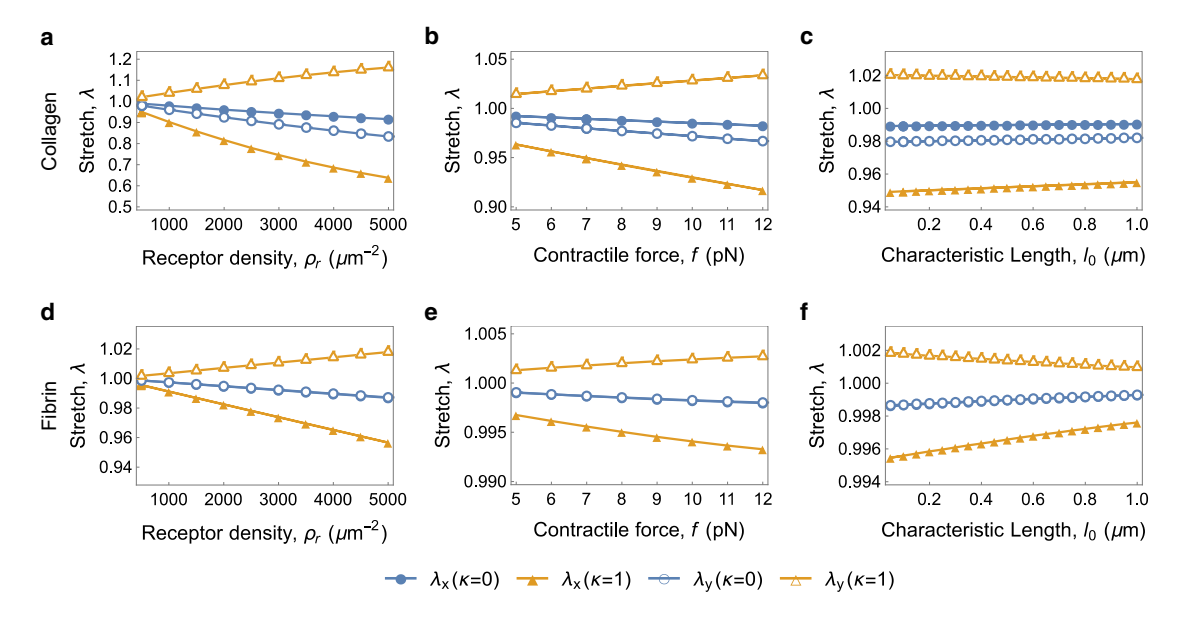


FIGURE 5 Homogeneous solutions of free gel contraction. Homogeneous domains with properties of either collagen or fibrin were allowed to contract freely under the active stress exerted by a cell population in the gel. Transmission of forces from the cell to the gel was given by the adhesion model. The stretches in x (filled markers) and y direction (unfilled markers) of isotropic gel (blue circles) and anisotropic gel primarily aligned in the x direction (orange triangles) varying with (a and b) receptor density ρ_r , (c and d) contractile force f, and (e and f) characteristic length l_0 were analyzed.

more contraction in a slightly nonlinear fashion due to the binding probability dependence on stretch. Increasing the characteristic length l_0 , or the distance between receptors (Fig. 5, c and f), suppressed contraction. The effects were larger on oriented gels with $\kappa = 1$ than on isotropic gels, and larger on collagen than on fibrin. Note that these contraction simulations were acute, i.e., no permanent gel remodeling was taken into consideration. Thus, the values of contraction were generally small. These curves were not calibrated against experimental data, but they did align qualitatively with experimental observations of gel contraction experiments (52–54) (see Table S2).

Finite element models of wound mechanobiology

Baseline simulations

Armed with the coupled adhesion model and description of the nonlinear mechanics of collagen and fibrin, we proceeded to simulate more representative tissue-scale problems with the use of a finite element model. The setup of the first simulation is illustrated in Fig. 6 a. To recapitulate cutaneous wound healing (25), we assigned collagen gel properties with slight anisotropy in the x direction to the blue healthy region in Fig. 6 b, and isotropic fibrin gel properties to the red wound region in Fig. 6 c. We applied the symmetry boundary conditions on the bottom and the left sides of the rectangular tissue domain, and stretched the other two sides with a biaxial deformation. The principal stresses of both the total stress and the active contribution generated by cells distributed at a density chosen from (31,39) are plotted in Fig. 6, d-k. Principal stresses increased with deformation, with greater stress in the stiff collagen domain compared with the soft fibrin domain, see Fig. 6 g. The active stress increased with stretch, as expected from the adhesion model results in Fig. 3. However, the influence of stretch was trivial in the healthy region occupied by the collagen gel because the collagen domain was very stiff. The stretch-mediated mechanosensing was more pronounced in the fibrin domain, with adhesion and active stress increasing as a function of stretch (Fig. 6, h-k).

The dynamic changes in the binding probability at the macroscale were also of interest to better understand the multiscale cross talk between tissue mechanics and adhesion kinetics. Fig. 6, l-o show the time evolution of the adhesion formation (an average response of the individual cell adhesion at a specific location in the finite element mesh). Adhesion binding probability equilibrated rapidly in collagen, but evolved more slowly in fibrin. The equilibrium probability was slightly larger in collagen compared with fibrin due to the contrasting stiffness of the two materials, which was expected based on the results in Fig. 3. The active stress field, Fig. 6, h-k, follows directly from the adhesion binding probability, as captured in Eq. 27.

Evolving cell densities

To better capture wound healing, we first considered changes in fibroblast density in the wound region. We changed the boundary conditions in Fig. 7 a, assuming that the wound was not under external tractions but rather subjected to fixed boundary conditions. As a consequence, the only stresses generated were a direct result of cell contractility. We only considered the hyperelastic equilibrium response. We used the volume fraction of fibroblasts

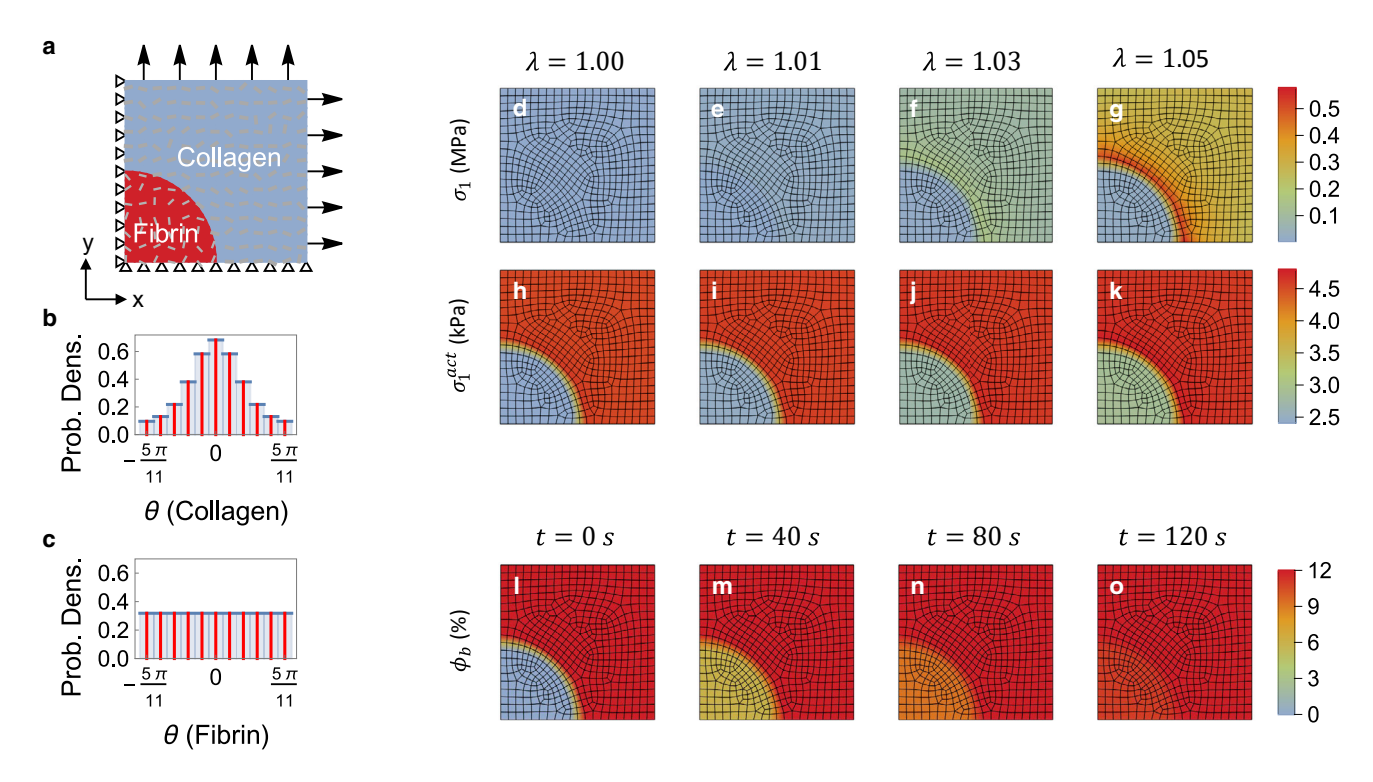


FIGURE 6 Active contraction at the beginning of wound healing. (a) The bottom and left sides of a collagen domain (blue) containing a fibrin inclusion (red) were set to be symmetric with respect to x and y axes, respectively. The whole tissue was under a biaxial tension. The healthy skin and wound domains were considered to be occupied by collagen and fibrin gels, respectively. (b) The collagen gel was slightly oriented in x direction by a von Mises distribution, as illustrated in Fig. 4 a ($\kappa = 1$). (c) The fibrin gel was isotropic ($\kappa = 0$). (d-k) The contours show the finite element results of total (d-g) and active (h-k) principal stress distributions under four different stretches ($\lambda = 1.00, 1.01, 1.03, 1.05$). (l-o) The time evolution of binding probability, i.e., the response of the individual cell adhesion model evaluated, at each integration point of the mesh.

 (ζ_c) to represent the cell density in the domain. To recapitulate wound healing (55), we assumed that fibroblast density in the wound region was initially less than that in the healthy region (Fig. 7 d). Then, as healing progressed, fibroblasts occupied the wound region, reaching values that were higher than in the healthy region (Fig. 7, e-g). The density of fibroblasts in the wound region that exceeded the density in the healthy region can be attributed to traveling wave solution (56). Finally, the density of fibroblasts in the wound reached the same value as in the surrounding tissue (Fig. 7 h). We computed the principal stresses of each stage in Fig. 7, i-m. As the wound was populated by fibroblasts, the active stress field resembled the cell density field (Fig. 7, n-r). However, even though there was a uniform cell density by the end time point, the active stress was not uniform due to the difference in material between the two domains (Fig. 7 r). As in the previous case, the active stress at the final step was fairly uniform in the two domains, whereas the total stress reflected the deformation of a stiff domain with a soft inclusion.

Transition in mechanical properties from fibrin to collagen

As wound healing progresses, the fibrin wound domain is replaced by a collagen-based ECM (57-60). Thus, to continue the refinement of our wound healing model, we started with the same configuration shown in Fig. 7 a, but considered a change in properties from fibrin to collagen at the center of the domain. The change in the strain energy density function from pure fibrin to pure collagen was based on the volume fraction of collagen ξ_{col} in the wound region, which was linearly changed from zero to one (Fig. 8 a). We considered the same cell density changes shown in Fig. 7, dh. As the fibrin domain turned to collagen, the strain state in the whole domain became more homogeneous (Fig. 8, b-k). The corresponding principal stress field is shown in the supporting material (Fig. S5). Permanent changes in fiber orientation were not considered in the current framework. As a result, the strain was not homogeneous in the final stage, despite that the cell density was uniform and the entire domain was made out of collagen. This implies that the mechanosensitive response of the fibroblasts may not return to the physiological state after wound healing unless both tissue composition and microstructure are remodeled. We also observed that, when the fibrin domain had no cells, the active stress in the surrounding region led to tensile strains in the wound (Fig. 8, b and g). As the cell density increased in the wound and the domain turned to collagen, the strains in the wound became compressive, indicative of wound contraction (Fig. 8, e and j). In addition, the anisotropy of the collagen domain led to anisotropic strains, with greater

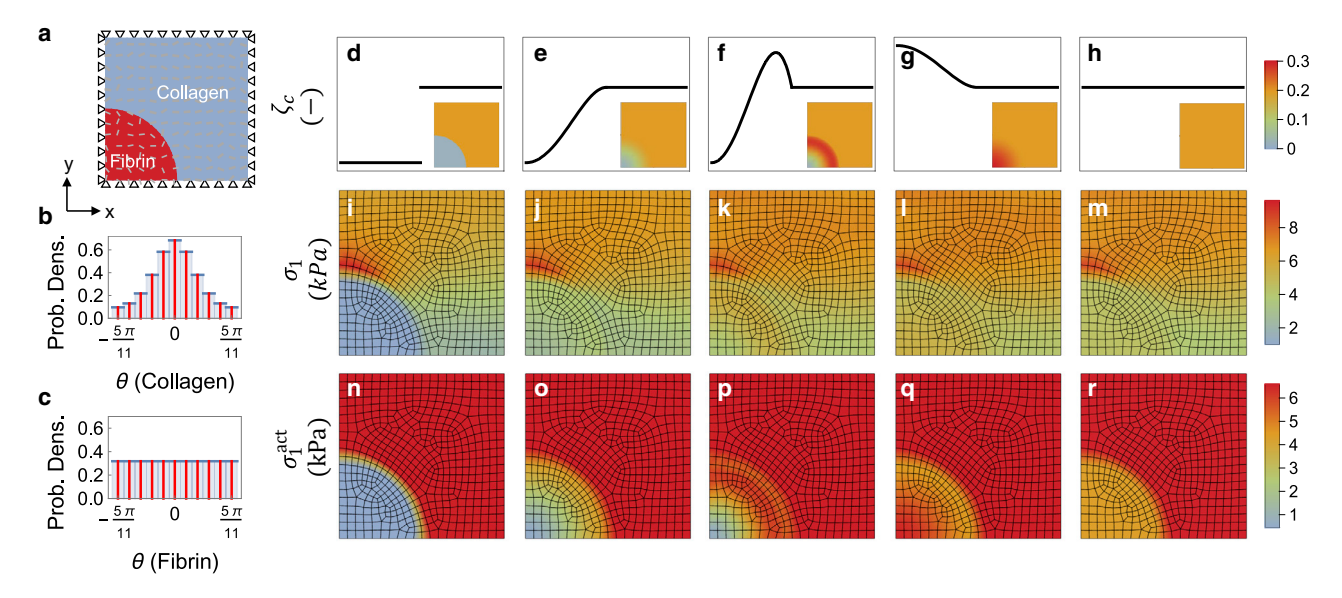


FIGURE 7 The effect of evolving fibroblast densities on stress distribution. (a) The same square tissue domain as Fig. 6 a was used, but the whole domain was fixed on all sides. (b and c) As in Fig. 6, the collagen fibers were slightly oriented ($\kappa = 1$) in the x direction and the fibrin gel was isotropic. (d-h) The lines and contours illustrate the radially distributed number of fibroblasts in the whole domain from the initial distribution where there were no fibroblasts in the wound (d) and the redistribution over the course of wound healing until there was a homogenous distribution across the wound (e-h). The lines show the relative cell density across the bottom of the square in (a), which is distributed radially. (i-r) The contours show the principal stress distributions of the total stress and active contribution

strains in the weaker y direction compared with the preferred collagen alignment in the x direction.

Increased contractility during wound healing

As a third example, we replaced the contractile force inside the wound by a higher value (Fig. 9 a), considering the contractility can be larger in the wound than that in the healthy region (57,61). We still considered the cell densities from Fig. 7, e–g, as well as the changes in collagen volume fraction from Fig. 8 a. As expected, the higher cell contractility increased the strains in the wound region. In particular, larger compressive strains (in terms of magnitude) were observed over a larger region in Fig. 9, f and g compared with Fig. 8, i and j. It also became clearer how the contraction of the wound started at the boundary (Fig. 9 e), and extended toward contraction of the entire wound region (Fig. 9 g).

DISCUSSION

To capture the macroscale mechanobiology of tissues based on mechanistic models of cell adhesion at the microscale, we progressively built more realistic simulations starting from a nonlinear model of fibrin and collagen mechanics, then coupling this model with Bell's model of adhesion, and finally linking the adhesion model to a tissue-level finite element framework through a two-way coupling. We used the model to simulate cutaneous wound healing incorporating the evolution of fibroblast density, the transition of mechanical properties of the wound, and effect of contractility. Continuum models of soft tissues, aided by the finite element method, are ideal to describe the biomechanics of complex biological systems at the macroscale, including wound healing (21,25,62–66). Yet, the vast majority of models at the tissue scale are based on phenomenological equations for cell mechanotransduction (67–69). On the other hand, celllevel mechanobiology models have also been developed, following the well-known model of cell adhesion proposed by Bell (6). These models are mostly limited to small scales and cannot explain the spatiotemporal mechanics of healing wounds at the tissue scale. In recognition of these limitations, multiscale coupling efforts have been recently reported. For example, in (70), the authors use an extension of Bell's model to solve for cell adhesion and spreading, and they also solve a finite element model of ECM deformation around a single fibroblast cell. Our work extends a recent version of Bell's model that considers linear viscoelastic behavior for individual ligand-receptor pairs to include the nonlinear mechanics of biopolymer fibers. This nonlinear adhesion model is then incorporated into a custom finite element implementation that couples cell adhesion kinetics to the nonlinear mechanics of tissues at the macroscale. The model demonstrates that the nonlinear mechanics of fibrin and collagen fibers naturally leads to stretch-driven mechanosensing at the cell scale (Fig. 3). Furthermore, when coupled to the finite element framework, the model captures how deformations applied at the tissue scale lead to the development of heterogeneous strains, stresses, and active contractile forces dependent on tissue composition and microstructure (Fig. 6).

Before deriving the extension of the adhesion model to the nonlinear mechanics regime, we ensured that the model

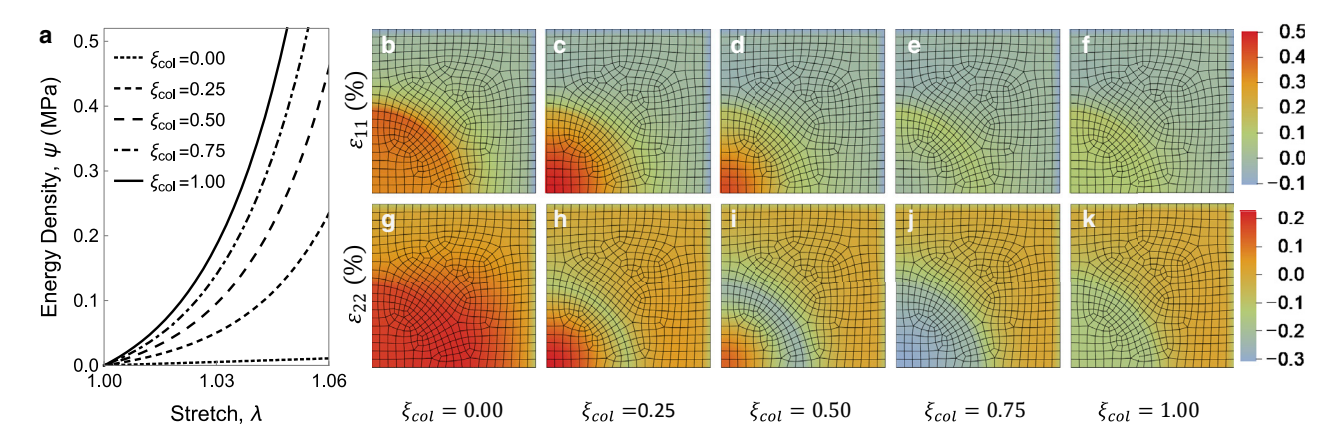


FIGURE 8 Effect of transition of wound domain from fibrin to collagen on strain. (a) The pseudo evolution of the strain energy density functions from fibrin gel ($\xi_{col} = 0$, dotted line) to collagen gels ($\xi_{col} = 1$, solid line), according to the volume fraction of collagen fibers in the wound region ξ_{col} . (b-k) The principal strain distributions with increasing collagen fibers in the wound region were analyzed, keeping the fibroblast distribution of each case as shown in Fig. 7, *d*–*h*.

could capture the linear elastic and linear viscoelastic cases described in the literature (7,8). We explored the adhesion response over the parameter space by varying stiffness, viscosity, and contractility. In line with experimental observations, the binding probability increased with increasing viscosity and stiffness of the ECM (9,71-73). The parameters for the individual bond kinetics, in particular the intrinsic association and dissociation rates, can vary by orders of magnitude depending on cell type and on the ECM substrate (7.8). Since we were primarily interested in fibroblasts, and fibrin and collagen substrates, we restricted our parameters to those scenarios as much as possible. A full list of parameter values and their sources from the literature are reported in Table S1.

Following our verification of the linear case (Fig. 2), we aimed to capture more realistic models of ECM mechanics using hyperelastic and hyper-viscoelastic frameworks. We introduced a new constitutive model that bridges the work of single-fiber mechanics (36,38) and tissue-level mechanics (33). This constitutive equation (Eq. 4) allowed us to fit experimentally determined individual fiber data (15,17), and the extension to biopolymer gels (Eq. 17) enabled fitting to fibrin and collagen gel data (15,17,46–48), as seen in Figs. 3, 4, and S2. One limitation of our proposed constitutive model is that it considers the biopolymer gels to be incompressible. However, collagen and fibrin gels show volume loss in uniaxial and biaxial tension (41). We explored the role of compressible material models in the supporting material but show the incompressible formulation in the main text because the compressible models exhibited large sensitivity to parameters and possible loss of convexity. In addition, the adhesion probability for the nonlinear cases, governed by Eqs. 7 and 8, depends on the in-plane response, which was fitted in Figs. 3 and S2.

The proposed models of fibrin and collagen fibers and gels were then used to study the differential effect of these materials on fibroblast adhesion. A simplifying assumption in the model was the use of constant contractile force in most of the simulations. More realistic scenarios include contractile force coupling to ECM stiffness as proposed by Cao et al. (74) and Walcott et al. (75). We implemented the force reinforcement model by Cao et al. and found that the effect of reinforcement had a large influence in the small deformation regime when the tangential stiffness of fibers was low, but the contractile force reached a constant value even at small stretches as the tangential stiffness of fibers increased (see Fig. S1). Therefore, we used constant values for the contractile force. With this assumption, we observed that the stiff collagen showed limited changes in cell adhesion with respect to stretch, but this was not the case for the comparatively soft fibrin substrate. The binding probability of cells to fibrin fibers was highly nonlinear, and stretch of collagen and fibrin fibers led to an increase in adhesion density. Thus, our model was able to predict cellular response to stretch using the well-established Bell's model by simply considering nonlinear ECM mechanics. To further investigate the transient behavior and possible role of more dynamic loading, we solved for adhesion over time at low and high prestretch of fibers and three different load rates. Lower loading rate initially led to higher adhesion probability, before equilibrating to the steady state, which depended only on the force value but not on the rate. These findings align with experimental observations (76).

Altered adhesion in stretched fibrin gels has been described previously (77). Fibroblasts on collagen gels have also shown increased adhesion in response to stretch (78,79). Our model did show increased adhesion on collagen with increasing stretch; however, the response was minimal. We hypothesize that the reason for the small response to stretch in collagen gels in our simulations stems from the lack of a mesoscale model of collagen mechanics. Recent work showed that fibrous soft collagen gels can produce an increased mechanosensitive response (increased adhesion) compared with fibrous stiff collagen gels, apparently contradicting previous experiments of fibroblasts cultured

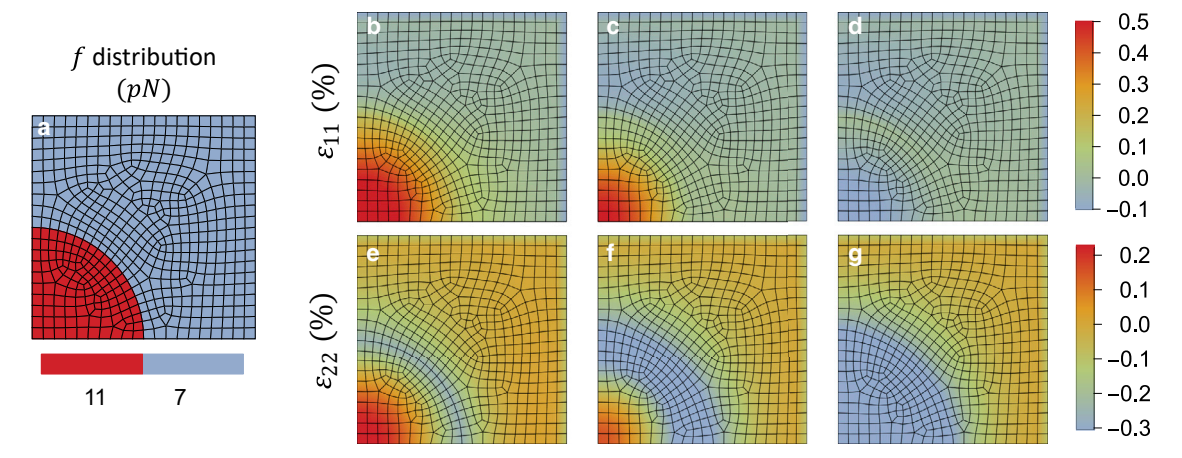


FIGURE 9 Different contractile forces in the wound region. (a) The wound region was under a higher contractile force (f = 11 pN) than that in the healthy region (f = 7 pN). (b-g) The distributed contractile forces were applied to the cases in Fig. 8, c-e and h-j, respectively. The contours show the results of strain field of each simulation.

on top of relatively homogeneous collagen gels of different stiffness (80,81). However, upon closer inspection, Balestrini and Billiar (82) found that fibroblasts on the fibrous gels were able to remodel the mesoscale fiber network in softer gels compared with stiffer gels, effectively changing the apparent stiffness sensed by the cells. Thus, for a mathematical model to capture the observations in (78,79,82), coupled models of cell adhesion to mesoscale mechanics are needed.

The parameters of the adhesion kinetics could have been tuned to induce a more pronounced mechanosensitive response of fibroblasts in collagen gels. However, rather than trying to arbitrarily modify the model or the parameters, we decided to keep the values obtained from the literature and reported in Table S1. Together, observations from the literature discussed above, and our results showing limited sensitivity of the adhesion model to collagen gel strains, point toward the need for an intermediate, mesoscale model of fibrin and collagen gels that accounts for the discrete fiber network mechanics. Models of the mechanics of fibrin and collagen gels using discrete fiber networks at the mesoscale have been developed (35–38,83), including our own work (66). Furthermore, we have coupled mesoscale models of fiber networks to finite element simulations at the tissue scale through the use of machine learning metamodels (64,84). However, the nonlinear adhesion model still needs to be coupled to the mesoscale model of fibrin and collagen gel mechanics, which is part of our ongoing work.

A two-way coupling between the mechanics of the ECM and the adhesion of fibroblasts was achieved by the introduction of an active contractile stress in Eq. 27. The active stress term has been used in other modeling contexts, such as other wound healing models (85), and remodeling of tissue engineering constructs (28). Our equation predicts forces by individual fibroblasts on collagen on the order of 26–44 nN for a contractile force of 7 pN (31) and 300 μ m⁻²(31) ligand density. This is within the range reported in (86,87), where a force of 11-52 nN per fibroblast was estimated experimentally. Similarly, our active stresses were in the range 2.4–4.6 kPa (Fig. 6, l-s), and traction force microscopy experiments of fibroblasts on collagen gels reported active stresses by single cells on the order of 0.353-4.14 kPa (39,88-91). The comparisons of the predicted values from our model with experimental data from literature are summarized in Table S2.

Finally, we implemented the nonlinear adhesion model into a custom finite element code and simulated the stress field of a fibrin wound inside a collagen domain. We did not model the entire wound healing process; rather, we started with a basic problem setup and gradually incorporated some of the evolving characteristics of the healing wound: evolving fibroblast distribution (Fig. 7), change in mechanical properties of the wound from fibrin to collagen (Fig. 8), and enhanced contractility of fibroblasts near the wound region (Fig. 9). Our simulations showed that, initially, fibroblasts in the collagen domain generated tensile stresses in the soft fibrin domain that actually distended the wound. As fibroblasts with enhanced contractility populated the wound domain and the composition changed from fibrin to collagen, the strains in the wound turned from tensile to compressive, i.e., they led to wound contraction (Figs. 8 and 9). This is in agreement with experiments and previous wound healing models (85,92,93). Thus, our finite element model shows promise for recapitulating the complex mechanobiology of wound healing, which has so far been restricted to phenomenological models at the tissue level (21,94).

More work is certainly needed to accurately model wound healing mechanobiology at multiple scales. Here, we developed a mechanistic model of fibroblast mechanobiology through a two-way coupling between nonlinear ECM deformation and fibroblast adhesion and contractile stress generation. However, the model currently lacks growth and remodeling, which is an essential part of wound healing and our ongoing efforts. While we based our model parameters on experimental data from the literature, and obtained results that are in agreement with previous observations and related computational models, additional experimental work is still needed.

CONCLUSIONS

In summary, we bridged a well-established cell-level adhesion model to the tissue-level mechanics of collagen and fibrin gels. To do so, we proposed a new constitutive equation that integrates previous work on single-fiber mechanics models and soft-tissue mechanics models. Consideration of the nonlinear hyper-viscoelastic behavior of collagen and fibrin naturally captured a mechanosensitive response in the adhesion model: stretch of fibers nonlinearly affected the energy at the adhesion and therefore the adhesion binding probability. The coupling is twofold: at the tissue level we considered the active contractile stress by fibroblasts, which is dependent on the solution of the cell-level adhesion model. We used our modeling framework to simulate wound healing accounting for the spatial evolution of fibroblast density, mechanical properties, and contractility, and observed wound contraction patterns in agreement with experiments and previous models.

SUPPORTING MATERIAL

Supporting material can be found online at https://doi.org/10.1016/j.bpj. 2022.01.012.

AUTHOR CONTRIBUTIONS

Y.G., A.B.T., and S.C. designed the research. Y.G. carried out all simulations, analyzed the data. Y.G., A.B.T., and S.C. wrote the article.

ACKNOWLEDGMENTS

This work was supported by the National Science Foundation under grant CMMI 1911346 to A.B.T. and S.C.

REFERENCES

- 1. Kim, S., M. Uroz, ..., C. S. Chen. 2021. Harnessing mechanobiology for tissue engineering. Dev. Cell. 56:180-191.
- 2. Tschumperlin, D. J., G. Ligresti, ..., V. H. Shah. 2018. Mechanosensing and fibrosis. J. Clin. Invest. 128:74-84.
- 3. Wozniak, M. A., K. Modzelewska, ..., P. J. Keely. 2004. Focal adhesion regulation of cell behavior. Biochim. Biophys. Acta. 1692:103-119.
- 4. Jahed, Z., H. Shams, ..., M. R. Mofrad. 2014. Mechanotransduction pathways linking the extracellular matrix to the nucleus. Int. Rev. Cell Mol. Biol. 310:171-220.
- 5. Humphrey, J. D., E. R. Dufresne, and M. A. Schwartz. 2014. Mechanotransduction and extracellular matrix homeostasis. Nat. Rev. Mol. Cell Biol. 15:802-812.
- 6. Bell, G. I. 1978. Models for the specific adhesion of cells to cells. Science. 200:618-627.
- 7. Chan, C. E., and D. J. Odde. 2008. Traction dynamics of filopodia on compliant substrates. Science. 322:1687-1691.

- 8. Gong, Z., S. E. Szczesny, ..., V. B. Shenoy. 2018. Matching material and cellular timescales maximizes cell spreading on viscoelastic substrates. Proc. Natl. Acad. Sci. U S A. 115:E2686-E2695.
- 9. Isenberg, B. C., P. A. Dimilla, ..., J. Y. Wong. 2009. Vascular smooth muscle cell durotaxis depends on substrate stiffness gradient strength. Biophys. J. 97:1313-1322.
- 10. Engler, A., L. Bacakova, ..., D. Discher. 2004. Substrate compliance versus ligand density in cell on gel responses. *Biophys. J.* 86:617–628.
- 11. Discher, D. E., P. Janmey, and Y. L. Wang. 2005. Tissue cells feel and respond to the stiffness of their substrate. Science. 310:1139-1143.
- 12. Chaudhuri, O., J. Cooper-White, ..., V. B. Shenoy. 2020. Effects of extracellular matrix viscoelasticity on cellular behaviour. Nature. 584:535-546.
- 13. Evans, E. A., and D. A. Calderwood. 2007. Forces and bond dynamics in cell adhesion. Science. 316:1148-1153.
- 14. Tonti, O. R., H. Larson, ..., S. Calve. 2021. Tissue-specific parameters for the design of ECM-mimetic biomaterials. Acta Biomater. 132:83–
- 15. Svensson, R. B., T. Hassenkam, ..., S. Peter Magnusson. 2010. Viscoelastic behavior of discrete human collagen fibrils. J. Mech. Behav. Biomed. Mater. 3:112-115.
- 16. Buehler, M. J., and S. Y. Wong. 2007. Entropic elasticity controls nanomechanics of single tropocollagen molecules. Biophys. J. 93:37-43.
- 17. Liu, W., C. R. Carlisle, ..., M. Guthold. 2010. The mechanical properties of single fibrin fibers. J. Thromb. Haemost. 8:1030–1036.
- 18. Helms, C. C., R. A. Ariëns, ..., M. Guthold. 2012. α - α cross-links increase fibrin fiber elasticity and stiffness. Biophys. J. 102:168-175.
- 19. Limbert, G. 2017. Mathematical and computational modelling of skin biophysics: a review. Proc. Math. Phys. Eng. Sci. 473:20170257.
- 20. Singer, A. J., and R. A. Clark. 1999. Cutaneous wound healing. N. Engl. J. Med. 341:738-746.
- 21. Tepole, A. B., and E. Kuhl. 2013. Systems-based approaches toward wound healing. Pediatr. Res. 73:553-563.
- 22. Freeman, J. W., and F. H. Silver. 2005. The effects of prestrain and collagen fibril alignment on in vitro mineralization of self-assembled collagen fibers. Connect. Tissue Res. 46:107-115.
- 23. Wang, N., I. M. Tolić-Nørrelykke, ..., D. Stamenović. 2002. Cell prestress. I. Stiffness and prestress are closely associated in adherent contractile cells. Am. J. Physiol. Cell Physiol. 282:C606-C616.
- 24. Ghibaudo, M., A. Saez, ..., B. Ladoux. 2008. Traction forces and rigidity sensing regulate cell functions. Soft Matter. 4:1836-1843.
- 25. Tepole, A. B. 2017. Computational systems mechanobiology of wound healing. Comput. Methods Appl. Mech. Eng. 314:46-70.
- 26. Montesano, R., and L. Orci. 1988. Transforming growth factor beta stimulates collagen-matrix contraction by fibroblasts: implications for wound healing. Proc. Natl. Acad. Sci. U S A. 85:4894–4897.
- 27. Hatami-Marbini, H., and M. R. K. Mofrad. 2010. Cytoskeletal mechanics and cellular mechanotransduction: a molecular perspective. In Cellular and Biomolecular Mechanics and Mechanobiology. Springer, pp. 3–27.
- 28. Loerakker, S., C. Obbink-Huizer, and F. P. T. Baaijens. 2014. A physically motivated constitutive model for cell-mediated compaction and collagen remodeling in soft tissues. Biomech. Model. Mechanobiol.
- 29. Schwarz, U. S., T. Erdmann, and I. B. Bischofs. 2006. Focal adhesions as mechanosensors: the two-spring model. *Biosystems*. 83:225–232.
- 30. Bangasser, B. L., S. S. Rosenfeld, and D. J. Odde. 2013. Determinants of maximal force transmission in a motor-clutch model of cell traction in a compliant microenvironment. Biophys. J. 105:581-592.
- 31. Sun, L., Q. H. Cheng, ..., Y. W. Zhang. 2009. Computational modeling for cell spreading on a substrate mediated by specific interactions, long-range recruiting interactions, and diffusion of binders. Phys. Rev. E Stat. Nonlin. Soft Matter Phys. 79:061907.

- 32. Huang, J., X. Peng, ..., J. Fang. 2011. Influence of substrate stiffness on cell-substrate interfacial adhesion and spreading: a mechano-chemical coupling model. J. Colloid Interface Sci. 355:503-508.
- 33. Holzapfel, G. A., T. C. Gasser, and R. W. Ogden. 2000. A new constitutive framework for arterial wall mechanics and a comparative study of material models. J. Elast. Phys. Sci. Solids. 61:1–48.
- 34. Liu, H., G. A. Holzapfel, ..., V. Prot. 2019. Anisotropic finite strain viscoelasticity: constitutive modeling and finite element implementation. J. Mech. Phys. Solids. 124:172-188.
- 35. Stylianopoulos, T., and V. H. Barocas. 2007. Volume-averaging theory for the study of the mechanics of collagen networks. Comput. Methods Appl. Mech. Eng. 196:2981-2990.
- 36. Lai, V. K., S. P. Lake, ..., V. H. Barocas. 2012. Mechanical behavior of collagen-fibrin co-gels reflects transition from series to parallel interactions with increasing collagen content. J. Biomech. Eng. 134:1.
- 37. Sander, E. A., V. H. Barocas, and R. T. Tranquillo. 2011. Initial fiber alignment pattern alters extracellular matrix synthesis in fibroblastpopulated fibrin gel cruciforms and correlates with predicted tension. Ann. Biomed. Eng. 39:714-729.
- 38. Aghvami, M., K. L. Billiar, and E. A. Sander. 2016. Fiber network models predict enhanced cell mechanosensing on fibrous gels. J. Biomech. Eng. 138:1010061-10100611.
- 39. Gaudet, C., W. A. Marganski, ..., J. Y. Wong. 2003. Influence of type I collagen surface density on fibroblast spreading, motility, and contractility. Biophys. J. 85:3329-3335.
- 40. Nicolas, A., B. Geiger, and S. A. Safran. 2004. Cell mechanosensitivity controls the anisotropy of focal adhesions. Proc. Natl. Acad. Sci. USA. 101:12520-12525.
- 41. Ban, E., H. Wang, ..., V. B. Shenoy. 2019. Strong triaxial coupling and anomalous Poisson effect in collagen networks. Proc. Natl. Acad. Sci. U S A. 116:6790-6799.
- 42. Brown, A. E., R. I. Litvinov, ..., J. W. Weisel. 2009. Multiscale mechanics of fibrin polymer: gel stretching with protein unfolding and loss of water. Science. 325:741-744.
- 43. Elosegui-Artola, A., R. Oria, ..., P. Roca-Cusachs. 2016. Mechanical regulation of a molecular clutch defines force transmission and transduction in response to matrix rigidity. Nat. Cell Biol. 18:540-548.
- 44. Elosegui-Artola, A., E. Bazellières, ..., P. Roca-Cusachs. 2014. Rigidity sensing and adaptation through regulation of integrin types. Nat. Mater. 13:631-637.
- 45. Thoumine, O., P. Kocian, ..., J. J. Meister. 2000. Short-term binding of fibroblasts to fibronectin: optical tweezers experiments and probabilistic analysis. Eur. Biophys. J. 29:398-408.
- 46. Seliktar, D., R. A. Black, ..., R. M. Nerem. 2000. Dynamic mechanical conditioning of collagen-gel blood vessel constructs induces remodeling in vitro. Ann. Biomed. Eng. 28:351-362.
- 47. Cross, V. L., Y. Zheng, ..., A. D. Stroock. 2010. Dense type I collagen matrices that support cellular remodeling and microfabrication for studies of tumor angiogenesis and vasculogenesis in vitro. Biomaterials. 31:8596-8607.
- 48. Jimenez, J., Y. Guo, ..., S. Calve. 2021. Macroscale mechanical characterization of het-erogeneous fibrin gels with varying density. In Proceedings of the 2021 Summer Biomechanics, Bioengineering and Biotransport Conference. Virtual Conference: SB3C, p. 803, isbn: 9781735180823. https://sb3c.org/2021-virtual-conference/programbook-proceedings-book/%7D.
- 49. Meador, W. D., G. P. Sugerman, ..., M. K. Rausch. 2020. The regionaldependent biaxial behavior of young and aged mouse skin: a detailed histomechanical characterization, residual strain analysis, and constitutive model. Acta Biomater. 101:403-413.
- 50. Hashimoto, K., N. Kajitani, ..., K. I. Matsumoto. 2018. Wound healing-related properties detected in an experimental model with a collagen gel contraction assay are affected in the absence of tenascin-X. Exp. Cell Res. 363:102–113.

- 51. Ferrenq, I., L. Tranqui, ..., P. Tracqui. 1997. Modelling biological gel contraction by cells: mechanocellular formulation and cell traction force quantification. Acta Biotheor. 45:267–293.
- 52. Ngo, P., P. Ramalingam, ..., G. T. Furuta. 2006. Collagen gel contraction assay. In Cell-Cell Interactions. Springer, pp. 103–109.
- 53. Sumiyoshi, K., A. Nakao, ..., H. Ogawa. 2003. Smads regulate collagen gel contraction by human dermal fibroblasts. Br. J. Dermatol. 149:464–470.
- 54. Tuan, T. L., and F. Grinnell. 1989. Fibronectin and fibrinolysis are not required for fibrin gel contraction by human skin fibroblasts. J. Cell. Physiol. 140:577-583.
- 55. McDougall, S., J. Dallon, ..., P. Maini. 2006. Fibroblast migration and collagen deposition during dermal wound healing: mathematical modelling and clinical implications. Philos. Trans. A Math. Phys. Eng. Sci. 364:1385-1405.
- 56. Tranquillo, R. T., and J. D. Murray. 1992. Continuum model of fibroblast-driven wound contraction: inflammation-mediation. J. Theor. Biol. 158:135-172.
- 57. Tomasek, J. J., G. Gabbiani, ..., R. A. Brown. 2002. Myofibroblasts and mechano-regulation of connective tissue remodelling. Nat. Rev. Mol. Cell Biol. 3:349-363.
- 58. Rouillard, A. D., and J. W. Holmes. 2014. Mechanical boundary conditions bias fibroblast invasion in a collagen-fibrin wound model. Biophys. J. 106:932-943.
- 59. Miron-Mendoza, M., J. Seemann, and F. Grinnell. 2008. Collagen fibril flow and tissue translocation coupled to fibroblast migration in 3D collagen matrices. Mol. Biol. Cell. 19:2051-2058.
- 60. Moreno-Arotzena, O., J. G. Meier, ..., J. M. García-Aznar. 2015. Characterization of fibrin and collagen gels for engineering wound healing models. Materials (Basel). 8:1636–1651.
- 61. Li, B., and J. H. Wang. 2011. Fibroblasts and myofibroblasts in wound healing: force generation and measurement. J. Tissue Viability. 20:108-
- 62. Ogawa, R., and D. P. Orgill. 2009. Mechanobiology of cutaneous wound healing and scarring. In Bioengineering Research of Chronic Wounds. Springer, pp. 31–42.
- 63. Makhsous, M., and F. Lin. 2009. A finite-element biomechanical model for evaluating buttock tissue loads in seated individuals with spinal cord injury. In Bioengineering Research of Chronic Wounds. Springer, pp. 181–205.
- 64. Lee, T., A. K. Gosain, ..., A. B. Tepole. 2019. Predicting the effect of aging and defect size on the stress profiles of skin from advancement, rotation and transposition flap surgeries. J. Mech. Phys. Solids. 125:572-590.
- 65. He, Y., D. Zuo, ..., S. Avril. 2019. Gradient-enhanced continuum models of healing in damaged soft tissues. Biomech. Model. Mechanobiol. 18:1443-1460.
- 66. Sree, V. D., and A. B. Tepole. 2020. Computational systems mechanobiology of growth and remodeling: integration of tissue mechanics and cell regulatory network dynamics. Curr. Opin. Biomed. Eng. 15:75-80.
- 67. Loerakker, S., T. Ristori, and F. P. T. Baaijens. 2016. A computational analysis of cell-mediated compaction and collagen remodeling in tissue-engineered heart valves. J. Mech. Behav. Biomed. Mater. 58:173-
- 68. Checa, S., M. K. Rausch, ..., G. N. Duda. 2015. The emergence of extracellular matrix mechanics and cell traction forces as important regulators of cellular self-organization. Biomech. Model. Mechanobiol. 14:1-13.
- 69. Song, D., N. Hugenberg, and A. A. Oberai. 2019. Three-dimensional traction microscopy with a fiber-based constitutive model. Comput. Methods Appl. Mech. Eng. 357:112579.
- 70. Pakshir, P., M. Alizadehgiashi, ..., B. Hinz. 2019. Dynamic fibroblast contractions attract remote macrophages in fibrillar collagen matrix. Nat. Commun. 10:1-17.

- 71. Dong, C., J. Cao, ..., H. H. Lipowsky. 1999. Mechanics of leukocyte deformation and adhesion to endothelium in shear flow. Ann. Biomed. Eng. 27:298-312.
- 72. Dong, C., and X. X. Lei. 2000. Biomechanics of cell rolling: shear flow, cell-surface adhesion, and cell deformability. J. Biomech. 33:35-43.
- 73. Elblbesy, M., and A. Hereba. 2009. Effect of viscosity and surface tension on erythrocytes adhesion. Curr. Appl. Phys. 9:872–874.
- 74. Cao, X., Y. Lin, ..., V. B. Shenoy. 2015. A chemomechanical model of matrix and nuclear rigidity regulation of focal adhesion size. Biophys. J. 109:1807-1817.
- 75. Walcott, S., D. H. Kim, ..., S. X. Sun. 2011. Nucleation and decay initiation are the stiffness-sensitive phases of focal adhesion maturation. Biophys. J. 101:2919-2928.
- 76. Chen, Y., J. Liao, ..., C. Zhu. 2019. Fast force loading disrupts molecular binding stability in human and mouse cell adhesions. Mol. Cell
- 77. Jansen, K. A., R. G. Bacabac, ..., G. H. Koenderink. 2013. Cells actively stiffen fibrin networks by generating contractile stress. Biophys. J. 105:2240-2251.
- 78. Madani, A., K. Garakani, and M. R. K. Mofrad. 2017. Molecular mechanics of Staphylococcus aureus adhesin, CNA, and the inhibition of bacterial adhesion by stretching collagen. PLoS One. 12:e0179601.
- 79. Omidvar, R., M. Tafazzoli-Shadpour, ..., M.-M. Khan. 2018. Quantifying effects of cyclic stretch on cell-collagen substrate adhesiveness of vascular endothelial cells. Proc. Inst. Mech. Eng. H. 232:531-541.
- 80. Baker, B. M., B. Trappmann, ..., C. S. Chen. 2015. Cell-mediated fibre recruitment drives extracellular matrix mechanosensing in engineered fibrillar microenvironments. Nat. Mater. 14:1262-1268.
- 81. Cao, X., E. Ban, ..., V. B. Shenoy. 2017. Multiscale model predicts increasing focal adhesion size with decreasing stiffness in fibrous matrices. Proc. Natl. Acad. Sci. U S A. 114:E4549-E4555.
- 82. Balestrini, J. L., and K. L. Billiar. 2009. Magnitude and duration of stretch modulate fibroblast remodeling. J. Biomech. Eng. 131:5.
- 83. Wang, H., A. S. Abhilash, ..., V. B. Shenoy. 2014. Long-range force transmission in fibrous matrices enabled by tension-driven alignment of fibers. Biophys. J. 107:2592-2603.

- 84. Lee, T., I. Bilionis, and A. B. Tepole. 2020. Propagation of uncertainty in the mechanical and biological response of growing tissues using multi-fidelity Gaussian process regression. Comput. Methods Appl. Mech. Eng. 359:112724.
- 85. Valero, C., E. Javierre, ..., M. J. Gómez-Benito. 2014. A cell-regulatory mechanism involving feedback between contraction and tissue formation guides wound healing progression. PLoS One. 9:e92774.
- 86. Harley, B. A., T. M. Freyman, ..., L. J. Gibson. 2007. A new technique for calculating individual dermal fibroblast contractile forces generated within collagen-GAG scaffolds. *Biophys. J.* 93:2911–2922.
- 87. Zahalak, G. I., J. E. Wagenseil, ..., E. L. Elson. 2000. A cell-based constitutive relation for bio-artificial tissues. Biophys. J. 79:2369-
- 88. Raman, P. S., C. D. Paul, ..., K. Konstantopoulos. 2013. Probing cell traction forces in confined microenvironments. Lab Chip. 13:4599-
- 89. Fu, J., Y. K. Wang, ..., C. S. Chen. 2010. Mechanical regulation of cell function with geometrically modulated elastomeric substrates. Nat. Methods, 7:733-736.
- 90. Legant, W. R., J. S. Miller, ..., C. S. Chen. 2010. Measurement of mechanical tractions exerted by cells in three-dimensional matrices. *Nat.* Methods, 7:969.
- 91. Yang, M. T., N. J. Sniadecki, and C. S. Chen. 2007. Geometric considerations of micro-to nanoscale elastomeric post arrays to study cellular traction forces. Adv. Mater. 19:3119-3123.
- 92. Javierre, E., P. Moreo, ..., J. M. García-Aznar. 2009. Numerical modeling of a mechano-chemical theory for wound contraction analysis. Int. J. Solids Struct. 46:3597-3606.
- 93. Mitrossilis, D., J. Fouchard, ..., A. Asnacios. 2009. Single-cell response to stiffness exhibits muscle-like behavior. Proc. Natl. Acad. Sci. U S A. 106:18243-18248.
- 94. Valero, C., E. Javierre, ..., M. J. Gómez-Benito. 2015. Challenges in the modeling of wound healing mechanisms in soft biological tissues. Ann. Biomed. Eng. 43:1654-1665.